bioRxiv preprint doi: https://doi.org/10.1101/2024.04.26.591372; this version posted April 29, 2024. The copyright holder for this preprint (which was not certified by peer review) is the author/funder, who has granted bioRxiv a license to display the preprint in perpetuity. It is made available under aCC-BY-NC-ND 4.0 International license.

Ancestral sequence reconstruction of Mic60 reveals a residue signature supporting respiration in yeast

Friederike M. C. Benning[1,2,7,*], Tristan A. Bell[1,2,4,7], Tran H. Nguyen[1,5,7], Della Syau[1,2,6], Louise B. Connell[3], Corrie J. B. daCosta[3], Luke H. Chao[1,2,8,**]

[1]Department of Molecular Biology, Massachusetts General Hospital, Boston, MA 02114, USA

[2]Department of Genetics, Harvard Medical School, Boston, MA 02115, USA

[3]Department of Chemistry and Biomolecular Sciences, University of Ottawa, Ottawa, Ontario K1N 6N5, Canada

[4]Present address: Generate Biomedicines, Somerville, MA 02143, USA

[5]Present address: Medical Scientist Training Program, Washington University in St. Louis, St. Louis, MO 63110, USA

[6]Present address: Biological and Biomedical Sciences Program, Harvard Medical School, Boston, MA 02115

[7]These authors contributed equally.

[8]Lead contact

*Correspondence: benning@molbio.mgh.harvard.edu

**Correspondence: chao@molbio.mgh.harvard.edu

bioRxiv preprint doi: https://doi.org/10.1101/2024.04.26.591372; this version posted April 29, 2024. The copyright holder for this preprint (which was not certified by peer review) is the author/funder, who has granted bioRxiv a license to display the preprint in perpetuity. It is made available under aCC-BY-NC-ND 4.0 International license.

Summary

In eukaryotes, the essential process of cellular respiration takes place in the cristae of mitochondria. The protein Mic60 is known to stabilize crista junctions; however, how the C-terminal Mitofilin domain of Mic60 mediates cristae-supported respiration remains elusive. Here, we used ancestral sequence reconstruction to generate Mitofilin ancestors up to and including the last opisthokont common ancestor (LOCA). We found that yeast-lineage derived Mitofilin ancestors as far back as the LOCA rescue respiration. By comparing Mitofilin ancestors with different respiratory phenotypes, we identify four residues that explain the difference between respiration functional yeast- and non-functional animal-derived common Mitofilin ancestors. Our results imply that Mitofilin-supported respiration in yeast stems from a conserved mechanism, and provide a foundation for investigating the divergence of candidate crista junction interactions present during the emergence of eukaryotes.

Keywords

Mic60, MICOS, Mitochondria, Cristae, Respiratory Chain, Ancestral Sequence Reconstruction

bioRxiv preprint doi: https://doi.org/10.1101/2024.04.26.591372; this version posted April 29, 2024. The copyright holder for this preprint (which was not certified by peer review) is the author/funder, who has granted bioRxiv a license to display the preprint in perpetuity. It is made available under aCC-BY-NC-ND 4.0 International license.

Introduction

Mitochondria are double membrane-defined eukaryotic organelles with essential metabolic and bioenergetic functions[1]. Cellular respiration, the process where adenosine triphosphate (ATP) is generated through oxidative phosphorylation, takes place in cristae, the characteristic invaginations of the inner mitochondrial membrane[2-5]. Within the inner mitochondrial membrane, a neck-like membrane structure called the crista junction connects cristae to the inner boundary membrane and is an important site for transit of substrates essential for respiration and other physiological functions[6-8].

Crista junction organization and stability is mediated by the mitochondrial contact site and crista organizing system (MICOS), a heterooligomeric inner mitochondrial membrane protein complex.[9-11] MICOS consists of two subcomplexes that assemble independently and have distinct roles in crista junction formation and stability[12-14]. In yeast, subcomplex I comprises Mic60 and Mic19 (and Mic25 in animals) and subcomplex II consists of Mic10, Mic26, Mic27, and Mic12 (Mic13 in animals), which connects the two subcomplexes[13,15].

Mic60 is the core shape-determining protein component of subcomplex I. It is conserved across eukaryotes, and all Mic60 proteins share a similar domain architecture with an N-terminal transmembrane helix followed by a large C-terminal region facing the intermembrane space[16]. Mic60 localizes at crista junctions, and together with Mic19, closely tethers the crista junction membrane to the outer mitochondrial membrane via interactions with the sorting and assembly machinery for β barrel proteins (i.e., SAM) and other membrane proteins.[11,17-20] Moreover, Mic60 is also an ancient MICOS component, with homologues identified in alphaproteobacteria, the extant cousins of a hypothesized endosymbiosed mitochondrial precursor[21]. Alphaproteobacterial Mic60 is found in intracytoplasmic membranes, which are functionally and morphologically analogous to mitochondrial cristae[16,22]. Bacterial and eukaryotic Mic60 share several functional and biophysical similarities, such as the ability to deform membranes[16,23].

bioRxiv preprint doi: https://doi.org/10.1101/2024.04.26.591372; this version posted April 29, 2024. The copyright holder for this preprint (which was not certified by peer review) is the author/funder, who has granted bioRxiv a license to display the preprint in perpetuity. It is made available under aCC-BY-NC-ND 4.0 International license.

Downregulation of Mic60 causes the loss of crista junctions[11,17,24], respiratory growth defects[25-28], and is a hallmark of several neurodegenerative disorders such as Parkinson's disease, Alzheimer's disease, and various myopathies[29-31]. It has been established that Mic60's most conserved region, its C-terminal Mitofilin domain, is important for respiration[26-28] and interacts with Mic19, Mic10, and Mic13[32-34]. Yet, how Mic60's Mitofilin sequence encodes its crista junction supported functions, in particular cellular respiration, remains unclear.

We used ancestral sequence reconstruction and respiratory growth assays to identify residues responsible for Mitofilin-supported yeast respiration[35]. In contrast to a previous report using a plasmid-based system, we observe that substitution of the yeast Mitofilin domain with human or alphaproteobacterial homologues at the endogenous locus does not rescue respiration[23]. To explore when Mic60's Mitofilin-supported respiration diverged, we reconstructed ancestral Mitofilin sequences and resurrected them for *in vivo* characterization. We found that common Mitofilin ancestors as far back as a putative last opisthokont common ancestor (LOCA) can rescue mitochondrial respiration in yeast. Comparing reconstructed ancestors with different rescue phenotypes, we identify four residues in the center of the Mitofilin fold that are involved in mitochondrial respiration. This finding, obtained from ancestral sequence reconstructions spanning an estimated one billion years of evolution[36], paves the way for molecular studies investigating the timing and sequence determinants of endosymbiotic interactions that drove eukaryogenesis.

bioRxiv preprint doi: https://doi.org/10.1101/2024.04.26.591372; this version posted April 29, 2024. The copyright holder for this preprint (which was not certified by peer review) is the author/funder, who has granted bioRxiv a license to display the preprint in perpetuity. It is made available under aCC-BY-NC-ND 4.0 International license.

Results

Re-defined domain boundaries for Mic60's Mitofilin domain

Despite extensive study, the definitions of Mic60's C-terminal Mitofilin domain boundary vary. While it has been established that the Mitofilin domain extends to the C terminus, multiple N-terminal boundaries have been proposed[10,26,34,37,38]. We superimposed AlphaFold2 predictions of Mic60 from *H. sapiens*, *S. cerevisiae* and the alphaproteobacterium *C. sphaeroides* and observed high structural conservation for a C-terminal region ranging from residues 318-540 (*S. cerevisiae* numbering; Figure 1A-C, Figure S1 for prediction confidence). This region extends beyond all previously assigned domain boundaries for the Mitofilin domain by an additional predicted 4-helix bundle in the N-terminal direction and includes the two previously proposed lipid binding sites (LBS 1 and LBS 2)[10,34,37] (Figure 1A). This newly defined Mitofilin domain is predicted to comprise two 4-helical bundles and an additional α helix α5, which contains most residues of the second previously assigned lipid binding site (LBS 2) and protrudes from the outer 4-helix bundle (Figure 1B, C). Residues of the other lipid binding site (LBS 1) are within the fourth α helix (α4) of the outer 4-helix bundle. Helix α8 spans both helical bundles. Based on these structural alignments, we redefined the Mitofilin domain boundaries, and used this revised Mitofilin definition (residues 318-540) in all subsequent experiments.

Alphaproteobacterial and human Mitofilin do not rescue cellular respiration in yeast

To test for Mic60 function, we applied an established respiratory growth assay in *S. cerevisiae* (Figure 2A). In this assay, oxidative phosphorylation-dependent respiratory growth was monitored using glycerol and ethanol (YPEG media; see Methods) as a non-fermentable carbon source. Only *S. cerevisiae* strains capable of cellular respiration can grow on YPEG. To control for mitochondria-independent growth deficits, we grew parallel cultures of all strains in dextrose (YPD media), a fermentable carbon source (Figure S2, Figure S3 for mitochondrial genome sequencing). We used CRISPR-Cas9 to generate Mic60 mutations at the endogenous locus in the genome of the S288C strain of *S. cerevisiae*. Consistent with previous work using derivatives of

bioRxiv preprint doi: https://doi.org/10.1101/2024.04.26.591372; this version posted April 29, 2024. The copyright holder for this preprint (which was not certified by peer review) is the author/funder, who has granted bioRxiv a license to display the preprint in perpetuity. It is made available under aCC-BY-NC-ND 4.0 International license.

BY4741 *S. cerevisiae*[26,28,37], we observe that knocking out Mic60 in *S. cerevisiae* (*mic60*Δ) leads to poor growth compared to wildtype under non-fermentable conditions (Figure 2A). Similarly, poor respiratory growth has been previously reported for C-terminally truncated versions of Mic60 ($Mic60_{1-140}$, $Mic60_{1-472}$, and $Mic60_{1-491}$ all show a reduced growth phenotype in *S. cerevisiae*)[26,28,37]. As expected, our truncation based on a more generous Mitofilin domain definition ($Mic60_{1-317}$; hereafter referred to as *mitofilin*Δ), also showed a reduced growth phenotype similar to *mic60*Δ (Figure 2A).

Given that the structural conservation of the Mitofilin domain extends beyond all major eukaryotic groups into prokaryotic alphaproteobacteria[38], we next asked whether Mitofilin-supported cellular respiration is similarly well conserved. We generated S288C strains where the *S. cerevisiae* Mitofilin sequence (residues 318-540) was swapped with that of Mitofilin homologues from different species at the endogenous locus. In contrast to previous reports[39], we found that a chimeric yeast strain encoding the alphaproteobacterial *C. sphaeroides* Mitofilin domain (residues 270-433; *mitofilin*Δ*::Mitofilin(C. sphaeroides)*) shows a similar growth deficit to the *mic60*Δ and *mitofilin*Δ strains on non-fermentable media (Figure 2A). Similarly, the yeast encoding the human Mitofilin chimera (residues 562-758; *mitofilin*Δ*::Mitofilin(H. sapiens)*) displays a respiratory growth deficit like *mic60*Δ (Figure 2A). Western blots of isolated mitochondrial fractions confirm the mitochondrial localization of *mitofilin*Δ and the chimeric *H. sapiens* Mitofilin and *C. sphaeroides* Mitofilin yeast strains (Figures S4). It is worth noting that a previous complementation study using plasmid-based expression observed a partial rescue of *S. cerevisiae* Mic60 function using the full-length *C. sphaeroides* Mic60 sequence[39]. In our work, we used CRISPR-Cas9 to generate chimeras of Mic60 at the endogenous locus of the *S. cerevisiae* genome.

K. phaffi Mitofilin rescues respiratory growth in *S. cerevisiae*

We noticed in alignments of eukaryotic Mic60 sequences that the *S. cerevisiae* Mitofilin domain contains a loop region (residues 364-406) between α helices α2 and α3, which is distinct to the Saccharomyceta clade (Figure 2B). To test whether this loop is important for yeast Mitofilin respiratory function, we generated a *S. cerevisiae* strain

bioRxiv preprint doi: https://doi.org/10.1101/2024.04.26.591372; this version posted April 29, 2024. The copyright holder for this preprint (which was not certified by peer review) is the author/funder, who has granted bioRxiv a license to display the preprint in perpetuity. It is made available under aCC-BY-NC-ND 4.0 International license.

that expresses a chimeric *S. cerevisiae* Mic60 with the Mitofilin domain of *K. phaffi* (residues 318-509; *mitofilin⊿::Mitofilin(K. phaffi)*), which lacks the unique loop region. We found that the Mic60 chimera with the *K. phaffi* Mitofilin domain localizes to mitochondria and grows like wildtype *S. cerevisiae* under non-fermentable conditions (Figure 2A, Figure S4). This indicates that despite only sharing 40% of sequence identity with *S. cerevisiae* Mitofilin (Figure 3B), the *K. phaffi* Mitofilin supports wildtype-like cellular respiration, and that the Saccharomyceta-specific loop region is not required for Mitofilin-supported respiratory growth in *S. cerevisiae*.

Ancestral sequence reconstruction of the last common opisthokont Mitofilin ancestors

Our finding that *K. phaffi* Mitofilin rescues respiratory growth in *S. cerevisiae* suggests the Mitofilin domain's role in cellular respiration may be an ancient function, well-conserved in yeast. To test this hypothesis and to determine an evolutionary time point when yeast Mitofilin respiratory function diverged in opisthokonts, we used ancestral sequence reconstruction[35] to infer the Mitofilin sequences of opisthokont ancestors, then tested the sufficiency for these ancestral Mic60 Mitofilin chimeras to support yeast respiratory growth. We began by collecting Mic60 sequences from all eukaryotic clades, optimizing for phylogenetic coverage of Ascomycota fungi, and truncated the sequences to only contain the C-terminal Mitofilin domain as defined above. Following multiple sequence alignments, we applied a stringent amino acid substitution model to generate Mitofilin-based molecular phylogenies (Figure 3A, Figure S5). Briefly, substitution models were sorted by Bayesian information criteria, and evaluated for their ability to achieve largely congruent evolutionary relationships between fungi (Figure S7). We found that the Q.yeast model[40,41] best modeled this tree, with +I and +G4 decorators chosen to approximate the evolutionary rate[42]. A yeast sequence-focused tree containing 121 sequences was then used to reconstruct ancestors along the fungal lineage from *S. cerevisiae* to the last common ancestors of Saccharomycotina (yLSCA), Ascomycota (yLACA), Fungi (yLFCA) and Opisthokonta (yLOCA) (Figure 3A-D). Reconstruction confidence is measured by the mean posterior probability for a reconstructed ancestor. We reconstructed 174-179 residues for yLSCA,

bioRxiv preprint doi: https://doi.org/10.1101/2024.04.26.591372; this version posted April 29, 2024. The copyright holder for this preprint (which was not certified by peer review) is the author/funder, who has granted bioRxiv a license to display the preprint in perpetuity. It is made available under aCC-BY-NC-ND 4.0 International license.

yLACA, yLFCA and yLOCA Mitofilin with a mean posterior probability ranging from 72% for yLOCA to 82% for yLACA and yLSCA (Figure 3C, Figures S7, S8).

We next reconstructed a tree with good phylogenetic coverage for animals to investigate the conservation of yeast respiratory function further down the lineage to the human Mitofilin domain (Figure 3A, Figures S6, S7). This phylogenetic tree focused on human lineage-derived reconstructed Mitofilin domains for the last vertebrate (hLVCA), last Bilateria non-arthropod (hLBnaCA), and last opisthokont common ancestor (hLOCA) (see methods for details). The mean posterior probability for hLVCA, hLBnaCA, and hLOCA ranged from 75-88% (Figure 3C, Figure S8). The yLOCA and hLOCA Mitofilin sequences share 64% sequence identify (Figure 3B).

Yeast-lineage derived Mitofilin LOCA rescues respiratory growth

To evaluate the functional conservation of the ancestor Mitofilin sequences, we generated yeast strains encoding Mitofilin chimeras of Mic60, where we exchanged the wildtype Mitofilin domain with the reconstructed ancestral Mitofilin domains. All the reconstructed yeast-derived ancestors localize to the mitochondria, as shown by immunoblots of mitochondrial fractions (Figure S4). Notably, all yeast ancestors (yLSCA, yLACA, yLFCA and yLOCA) grow like wildtype in respiratory media (Figure 3D, Figure S9). To better quantify yeast respiratory growth over time, we cultured yeast strains in liquid medium (50 ml YPEG) under non-fermentable conditions and assayed cell density by spectrophotometrically measuring the OD_{600} at defined time points. We observe two growth regimes: while growth rates do not significantly differ within the first 24 hours of growth, during mid-log phase, all yeast ancestors and *K. phaffi* Mitofilin grow like wildtype, whereas *mic60*Δ and *mitofilin*Δ show a significantly reduced growth rate, which is consistent with colony number and thickness in the solid growth assays (Figure 3D, Figure 2 for *K. phaffi*). Our findings suggest that Mitofilin's respiratory growth function in yeast is conserved all the way to yLOCA, covering over one billion years of evolution[43].

bioRxiv preprint doi: https://doi.org/10.1101/2024.04.26.591372; this version posted April 29, 2024. The copyright holder for this preprint (which was not certified by peer review) is the author/funder, who has granted bioRxiv a license to display the preprint in perpetuity. It is made available under aCC-BY-NC-ND 4.0 International license.

Whole genome sequencing confirms the correct genomic insertion of the human-lineage derived ancestor sequences in the yeast strain; however, we do not observe stable expression for the human-derived hLBnaCA and hLOCA ancestors in immunoblots (Figure S4). Accordingly, the human-lineage derived ancestors show deficient respiratory growth like *mic60*Δ (Figure 3D, Figure S9). While the hLVCA Mitofilin ancestor expresses and localizes to mitochondria (Figure S4), it does not rescue respiratory growth (Figure S9).

Structural comparison of ancestors

Ancestral sequence reconstruction infers the amino acid sequences of putative ancestors, which we compared to identify residue signatures that correlate with function. We first generated structure predictions of Mitofilin ancestors using our reconstructed sequences as input for AlphaFold2. As expected based on sequence identity, all predicted structures adopt the same overall fold (Figure 3E). To identify potential amino acids responsible for functional differences, we analyzed multiple sequence alignments of extant and resurrected Mitofilin sequences for similarities in functional constructs in yeast (wildtype, *K. phaffi* and all yeast-lineage derived ancestral sequences), and differences compared with constructs that exhibited a *mic60*Δ-like growth phenotype (*H. sapiens* and all human-lineage derived ancestors) or constructs that did not stably express (hLOCA, hLBnaCA). We refer to functional constructs as all extant and reconstructed sequences that show wildtype-like respiratory growth and refer to non-functional constructs as sequences that exhibit a *mic60*Δ-like respiratory growth curve or sequences that do not show stable expression in yeast (Figure 3D, Figures S4, S9).

We identified four residues in the Mitofilin domain, which are either identical or retain similar chemical properties (charge, hydrophobicity, size) in all functional constructs, but differ in the non-functional constructs (Figure 4A, B, Figure S10). Intriguingly, when mapped onto the predicted structure, these four residues are located in a line that runs across the center of the Mitofilin domain, perpendicular to the helical bundle axis (Figure 4B). Two of these residues, Glycine 421 (*S. cerevisiae* nomenclature) and Leucine 425 are positioned on the loop between helices α3 and α4, which connects the predicted

bioRxiv preprint doi: https://doi.org/10.1101/2024.04.26.591372; this version posted April 29, 2024. The copyright holder for this preprint (which was not certified by peer review) is the author/funder, who has granted bioRxiv a license to display the preprint in perpetuity. It is made available under aCC-BY-NC-ND 4.0 International license.

inner and outer 4-helix bundles of the Mitofilin domain (Figure 4B). Glycine 421 changes from a small (Glycine) or hydrophilic (Serine/Asparagine) residue in all functional sequences into a charged residue (Glutamate) in all human-derived ancestors. Notably, Glycine 421 corresponds to a Threonine (Threonine 622) in *H. sapiens*. Leucine 425 is a hydrophobic residue (Leucine/Alanine) in all yeast constructs, but a polar amino acid (Serine/Tyrosine) in all non-functional sequences. Aspartate 497 on α7 on the outer 4-helix bundle is a negatively charged or small polar residue (Aspartate/Glutamate/Serine) in functional constructs. In non-functional constructs, Aspartate 497 is a larger polar or a hydrophobic amino acid (Asparagine/Glutamine/Leucine). The fourth residue which differs between functional and non-functional residues, Arginine 522, is located on helix α8 and exists as a positively charged residue in functional sequences (Arginine/Lysine), and a hydrophobic residue (Alanine/Leucine/Methionine) in non-functional constructs.

bioRxiv preprint doi: https://doi.org/10.1101/2024.04.26.591372; this version posted April 29, 2024. The copyright holder for this preprint (which was not certified by peer review) is the author/funder, who has granted bioRxiv a license to display the preprint in perpetuity. It is made available under aCC-BY-NC-ND 4.0 International license.

Discussion

Respiration is an essential function supported by mitochondrial cristae. While the essentiality of Mic60 for stable crista junctions is established[26,28,37], understanding of conserved sequence and structural determinants for cristae-supported respiration have been lacking. Here we used ancestral sequence reconstruction to infer putative Mic60 Mitofilin sequences along the fungal lineage from *S. cerevisiae* to the last opisthokont common ancestor (LOCA). We show that Mic60 Mitofilin ancestors as far back as the last opisthokont common ancestor (yLOCA) rescue yeast mitochondrial respiration. These results indicate that Mitofilin-supported respiration is based on a well-conserved mechanism, spanning approximately one billion years of evolutionary history. This observation is striking, given the high rate of Mitofilin evolution in fungi, as indicated by the number of residue substitutions in the yeast phylogenetic tree compared to that of animals. An implication of this finding is that respiration-supporting interactions between the Mitofilin domain and partner proteins may also be similarly well-conserved.

Previously, Tarasenko *et al.* reported a “slight” rescue of yeast respiratory growth by plasmid-expressed and mitochondrially targeted wildtype C-terminally FLAG-tagged full-length alphaproteobacterial Mic60[39]. In contrast, when introducing the Mitofilin domain of the same alphaproteobacterial species as a yeast chimera at the endogenous locus with CRISPR-Cas9, we observe a definitive *mic60*Δ-like respiratory growth deficit. Since Mic60 function is coupled to its expression levels[29,31], we opted for genome editing by CRISPR-Cas9 at the endogenous locus, as opposed to plasmid-based expression to avoid plasmid-specific protein expression effects. Furthermore, despite confirmation of correct insertion by whole-genome sequencing, two yeast Mic60 chimeras with human-lineage derived Mitofilin ancestors do not show protein expression (Figure S4). Accordingly, these Mic60 chimeras also display a *mic60*Δ-like respiratory growth phenotype (Figure 3D, Figure S9). Since the expressed and non-expressed yeast Mic60 chimeras all contain the N-terminal mitochondrial targeting sequence and only differ in the C-terminal Mitofilin domain (Figure 1A), these observations suggest that additional, yet to be defined, mechanisms of proteostasis are at play.

bioRxiv preprint doi: https://doi.org/10.1101/2024.04.26.591372; this version posted April 29, 2024. The copyright holder for this preprint (which was not certified by peer review) is the author/funder, who has granted bioRxiv a license to display the preprint in perpetuity. It is made available under aCC-BY-NC-ND 4.0 International license.

Being a probabilistic approach, ancestral sequence reconstruction includes an inherent degree of uncertainty, even with the most robust reconstructions. By correlating respiratory growth profiles with the corresponding amino acid sequences, we were able to identify just four residues that explain the difference in Mitofilin function for yeast- and animal-derived ancestors. This is an advance over previous structure/function dissections of the Mitofilin domain that mainly used various truncation constructs[26,28,37]. These residues differ in chemical properties in functional and non-functional constructs. Interestingly, these residues are in close proximity to one another, within a central axis of the Mitofilin domain, perpendicular to the two distinctive 4-helix bundles. Given Mic60's functions, candidate roles for these residues may include domain stability, self-assembly, or protein-protein interactions. While it has been observed that Mic60's Mitofilin domain interacts with several proteins, knowledge on binding interfaces is sparse[32-34]. By identifying single candidate residues, this work lays the foundation for future work investigating mechanistic details of Mitofilin-supported respiration.

Limitations of the study

This study identifies conserved sequence elements in Mic60's Mitofilin domain that are important for yeast respiration. This work does not explore whether these residues complement other organelle functions, nor does this study investigate the role for these residues in animal cells. This work focused on the C-terminal Mitofilin domain of Mic60 due to its extreme conservation through eukaryotes, which is requisite for the ancestral sequence reconstruction approach. The role for other portions of Mic60, or other components of MICOS were not investigated. These interesting questions provide promising avenues for future investigation.

bioRxiv preprint doi: https://doi.org/10.1101/2024.04.26.591372; this version posted April 29, 2024. The copyright holder for this preprint (which was not certified by peer review) is the author/funder, who has granted bioRxiv a license to display the preprint in perpetuity. It is made available under aCC-BY-NC-ND 4.0 International license.

Acknowledgments

We thank L. Stirling Churchman for gifting us the S288c DBY12045 yeast strain; Ulandt Kim and the NextGen Sequencing Core at MGH for their outstanding support; Andrew J. Roger and Sergio A. Muñoz-Gómez for helpful discussions and advice. We acknowledge support from the Swiss National Science Foundation grant P180777 (F.M.C.B.), the Keystone Future of Science Fund (F.M.C.B), the Helen Hay Whitney Foundation (T.A.B.), Natural Sciences and Engineering Research Council of Canada grant RGPIN-2016-04801 (C.J.B.d.C.), Canada Foundation for Innovation grant 34475 (C.J.B.d.C.), Canadian Institutes of Health Research grant 377068 (C.J.B.d.C.), New Frontiers in Research Fund-Exploration grant NFRFE-2018-00064 (C.J.B.d.C.), the Moore–Simons Project on the Origin of the Eukaryotic Cell grant 9736 (L.H.C., C.J.B.d.C.) and National Institutes of Health grant R35GM142553 (L.H.C.).

Author Contributions

F.M.C.B., T.A.B., T.H.N., D.S. and L.H.C. conceived of the study and designed the experiments. F.M.C.B., T.A.B., T.H.N. and D.S. generated the yeast strains. F.M.C.B. and T.H.N. performed growth assays and mitochondrial localization experiments. T.A.B., T.H.N, L.B.C and C.J.B.d.C. performed ancestral sequence reconstruction. F.M.C.B., T.A.B., T.H.N., C.J.B.d.C., and L.H.C. analyzed the data. F.M.C.B. and T.A.B. created figures and tables, and F.M.C.B. and L.H.C. wrote the manuscript with contributions from T.A.B. and T.H.N. All authors approved the final version of the manuscript.

Declaration of Interests

The authors declare no competing interests.

bioRxiv preprint doi: https://doi.org/10.1101/2024.04.26.591372; this version posted April 29, 2024. The copyright holder for this preprint (which was not certified by peer review) is the author/funder, who has granted bioRxiv a license to display the preprint in perpetuity. It is made available under aCC-BY-NC-ND 4.0 International license.

Figures

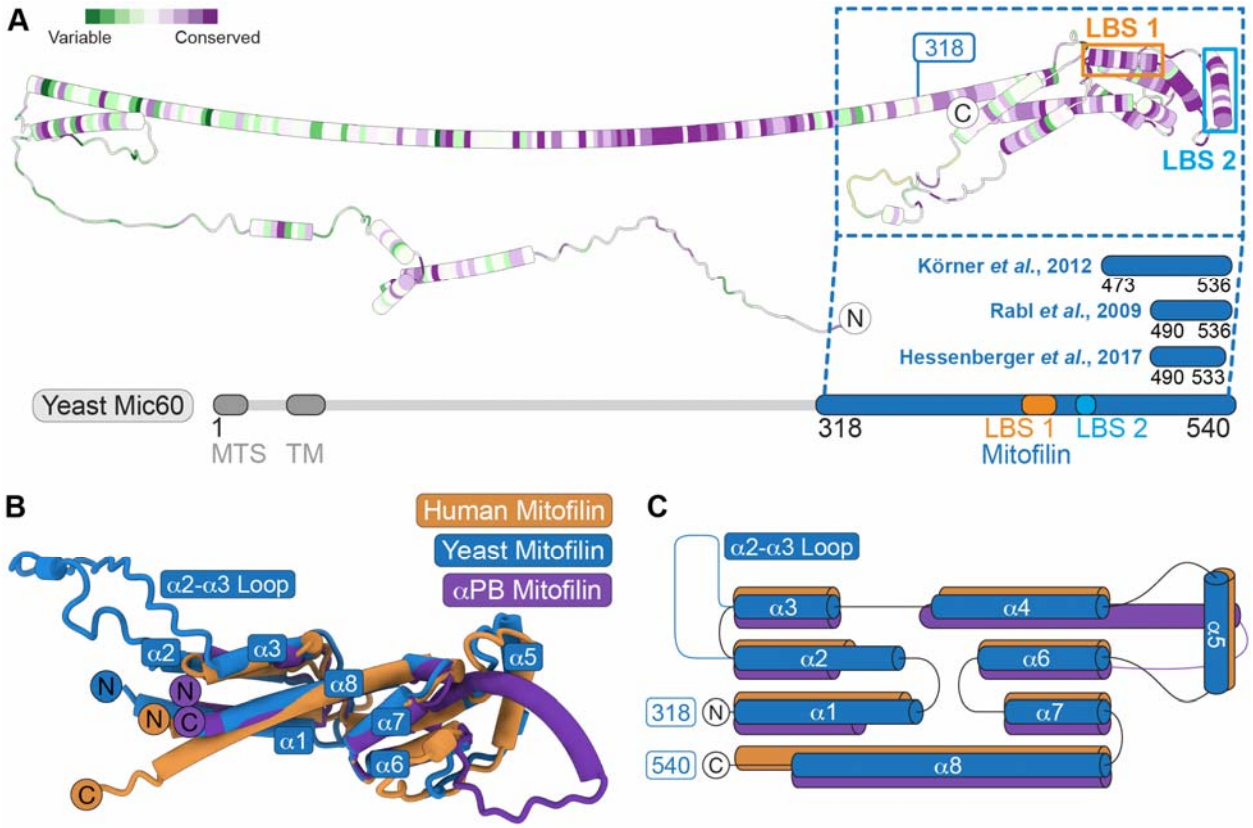

Figure 1. Boundaries of Mic60's C-terminal Mitofilin domain defined based on its structural conservation.

(A) Sequence conservation mapped onto the AlphaFold2-predicted *S. cerevisiae* Mic60 structure (AF-P36112-F1) using the ConSurf webserver[46,47]. Conservation is represented by a normalized conservation score, indicating relative sequence conservation at each residue compared to the entire protein chain. Variable residues are shown in green and conserved residues are shown in purple. Previously published experimentally determined Mitofilin domain boundaries are indicated as blue bars above the linear Mic60 polypeptide scheme: residues Körner *et al.*[36], Rabl *et al.*[10], Hessenberger *et al.*[34] MTS: mitochondrial targeting sequence; TM: transmembrane region; LBS 1 and LBS 2: lipid binding sites 1 and 2[34].

(B) Superposition of AlphaFold2-predicted structures of the yeast (blue; residues 318-540), human (gold; residues 562-758) and alphaproteobacterial (purple; residues 270-433) Mitofilin domains. RMSD by residue values for superposition on the yeast Mitofilin

bioRxiv preprint doi: https://doi.org/10.1101/2024.04.26.591372; this version posted April 29, 2024. The copyright holder for this preprint (which was not certified by peer review) is the author/funder, who has granted bioRxiv a license to display the preprint in perpetuity. It is made available under aCC-BY-NC-ND 4.0 International license.

domain: 1.04 Å for human Mitofilin (Uniprot ID: Q16891) relative to yeast, 0.92 Å for alphaproteobacterial Mitofilin (Uniprot ID: B9KRE6) relative to yeast. Sequences used for AlphaFold2 structure prediction are listed in Table S1. αPB: alphaproteobacterial.

(C) Topology diagram of the human (gold), yeast (blue) and alphaproteobacterial (purple) Mitofilin domain. Domain boundaries for yeast Mic60 Mitofilin are listed next to the N and C terminus.

bioRxiv preprint doi: https://doi.org/10.1101/2024.04.26.591372; this version posted April 29, 2024. The copyright holder for this preprint (which was not certified by peer review) is the author/funder, who has granted bioRxiv a license to display the preprint in perpetuity. It is made available under aCC-BY-NC-ND 4.0 International license.

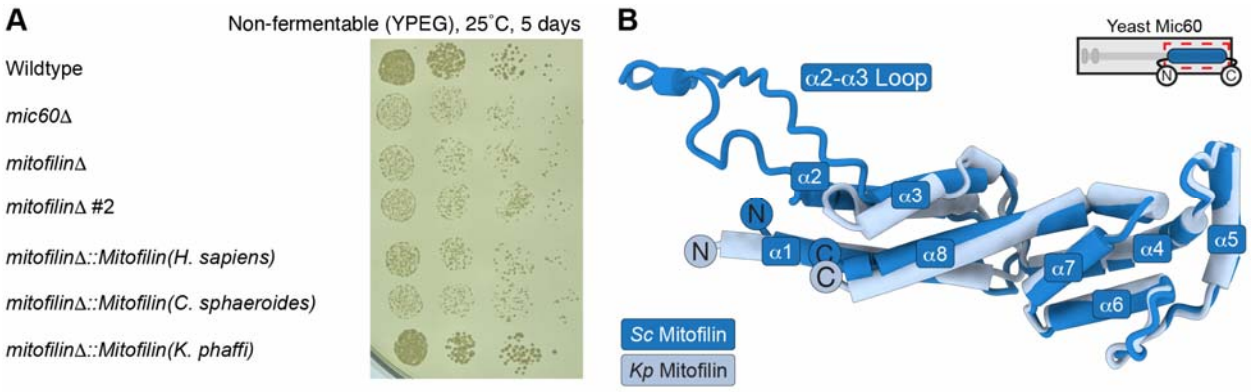

Figure 2. Respiratory growth phenotypes for yeast Mic60 Mitofilin chimeras.

(A) Spot assay of yeast Mic60 chimeric strains on YPEG media, which is non-fermentable for yeast, after 5 days at 25˚C. Deletion of the Mitofilin domain (*mitofilin*Δ and *mitofilin*Δ *#2,* which is the same strain as *mitofilin*Δ but a differerent colony) in yeast Mic60 or substituting it with the *H. sapiens* (*mitofilin*Δ*::Mitofilin(H. sapiens)*) and the *C. sphaeroides* (*mitofilin*Δ*::Mitofilin(C. sphaeroides*) Mitofilin domain results in knockout-like (*mic60*Δ) colony density and sizes. Yeast Mic60 with the *K. phaffi* Mitofilin domain (*mitofilin*Δ*::Mitofilin(K. phaffi*) exhibits wildtype-like growth.

(B) Superposition of AlphaFold2-predicted models of the *S. cerevisiae* Mitofilin domain (dark blue) and the *K. phaffi* Mitofilin domain (light blue) to highlight the extended Saccharomyceta clade loop region ('α2-α3 Loop') connecting helices α2 and α3.

bioRxiv preprint doi: https://doi.org/10.1101/2024.04.26.591372; this version posted April 29, 2024. The copyright holder for this preprint (which was not certified by peer review) is the author/funder, who has granted bioRxiv a license to display the preprint in perpetuity. It is made available under aCC-BY-NC-ND 4.0 International license.

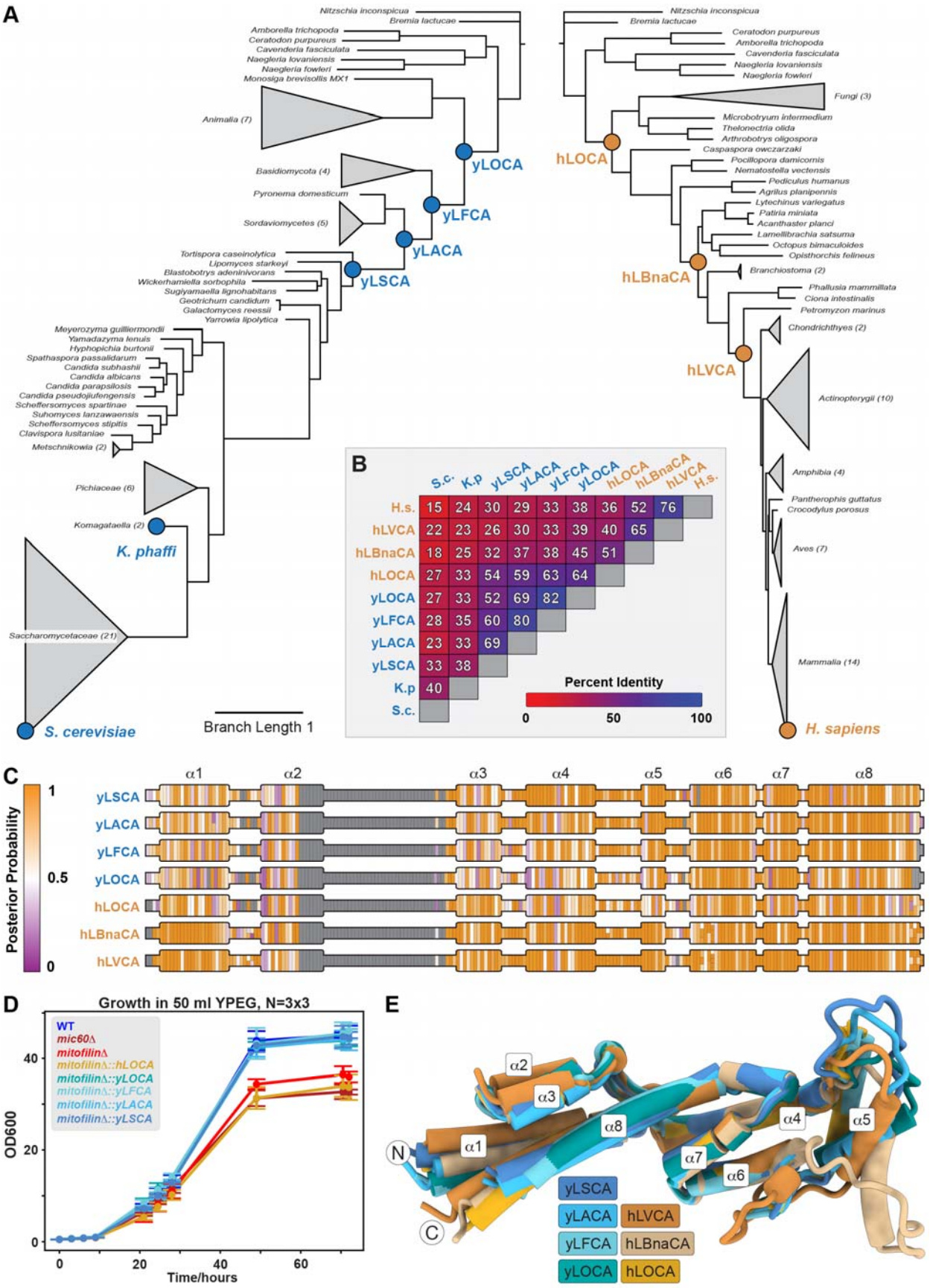

bioRxiv preprint doi: https://doi.org/10.1101/2024.04.26.591372; this version posted April 29, 2024. The copyright holder for this preprint (which was not certified by peer review) is the author/funder, who has granted bioRxiv a license to display the preprint in perpetuity. It is made available under aCC-BY-NC-ND 4.0 International license.

Figure 3. Ancestral sequence reconstruction of Mitofilin domains.

(A) Yeast-focused (left) and animal-focused (right) phylogenies of the Mitofilin domain used for ancestral sequence reconstruction. Reconstructed nodes are designated by colored spheres (blue: yeast-derived ancestors; gold: animal-derived ancestors). Trees are scaled to identical branch lengths. Some clades are collapsed for clarity. Full trees with branch supports can be found in Figures S5 and S6. yLxCA: yeast-derived last common ancestor, hLxCA: human-derived last common ancestor, LSCA: last Saccharomycotina common ancestor, LACA: last Ascomycota common ancestor, LFCA: last Fungi common ancestor, LOCA: last ophisthokont common ancestor, LVCA: last vertebrate common ancestor, LBnaCA: last Bilateria non-arthropod common ancestor.

(B) Table showing pairwise sequence identity (in %) between each extant or reconstructed ancestral Mitofilin domain. Pairwise sequence identify is colored from red (low) to blue (high).

(C) Linear topology schemes of reconstructed ancestors color-coded per residue by posterior probability. Posterior probability is colored from purple (low) to orange (high). Gray residues indicate absent residues in the reconstructed ancestor. Secondary structure elements (helices α1 to α8) are represented by protuberant regions.

(D) Growth curve for wildtype yeast Mic60 (WT, blue), *mic60*Δ (dark red), *mitofilin*Δ (bright red), and reconstructed Mitofilin ancestors cultivated under respiratory conditions (50 ml YPEG; N = 9).

(E) Superposition of AlphaFold2 models of reconstructed ancestors (dark blue: yLSCA; sky blue: yLACA; light blue: yLFCA, teal: yLOCA; gold: hLOCA; light brown: hLBnaCA; dark brown: hLVCA).

bioRxiv preprint doi: https://doi.org/10.1101/2024.04.26.591372; this version posted April 29, 2024. The copyright holder for this preprint (which was not certified by peer review) is the author/funder, who has granted bioRxiv a license to display the preprint in perpetuity. It is made available under aCC-BY-NC-ND 4.0 International license.

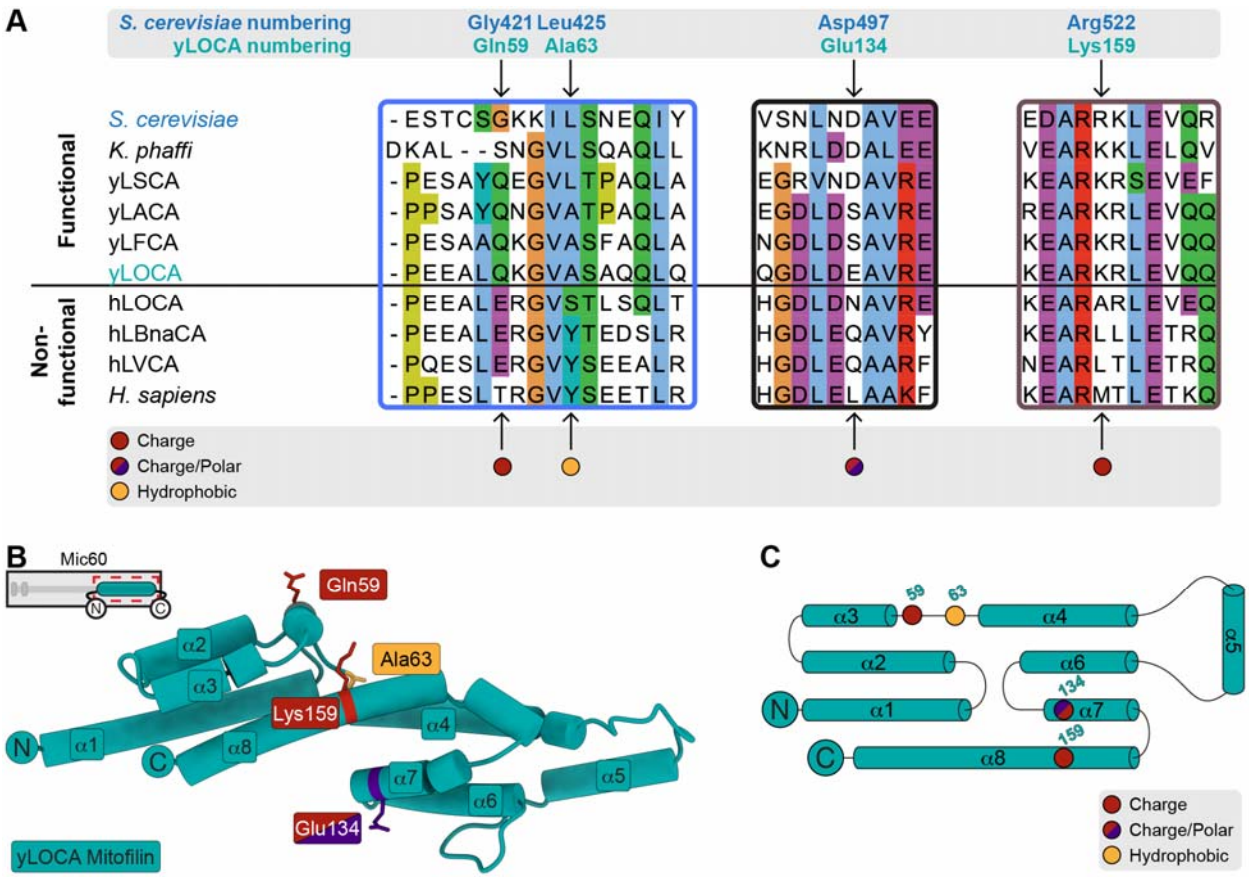

Figure 4. Four candidate residues can explain functional differences between Mitofilin ancestors.

(A) Contextualized regions of multiple sequence alignment between *S. cerevisiae*, *K. phaffi*, *H. sapiens*, and resurrected ancestor Mitofilin domains. Respiration functional and non-functional sequences are highlighted as such and separated by a horizontal black line. Four residues that could explain respiratory growth phenotypes are indicated by arrows with *S. cerevisiae* and yLOCA numbering listed above the alignment. Chemical properties of the four candidate residues in yeast and yeast-derived ancestors relative to human and animal-derived ancestors are denoted by colored spheres below the alignment (red sphere: change in charge; red/purple sphere: changes in charge and polar nature; yellow sphere: change in hydrophobicity). Colored boxes in alignment correspond to colored boxes in full alignment in Figure S10.

(B) Candidate residues that can explain differences in respiratory phenotypes between yeast-derived and animal-derived Mitofilin ancestors are mapped onto the AlphaFold2 predicted yLOCA model. Residues are numbered by yLOCA nomenclature (see (A) for

bioRxiv preprint doi: https://doi.org/10.1101/2024.04.26.591372; this version posted April 29, 2024. The copyright holder for this preprint (which was not certified by peer review) is the author/funder, who has granted bioRxiv a license to display the preprint in perpetuity. It is made available under aCC-BY-NC-ND 4.0 International license.

conversion to *S. cerevisiae* numbering) and colored by their chemical properties as described in (A). All four residues map to the central area of the Mitofilin domain.

(C) Topology diagram of yLOCA showing the location of the four candidate residues, which are colored by their chemical properties.

bioRxiv preprint doi: https://doi.org/10.1101/2024.04.26.591372; this version posted April 29, 2024. The copyright holder for this preprint (which was not certified by peer review) is the author/funder, who has granted bioRxiv a license to display the preprint in perpetuity. It is made available under aCC-BY-NC-ND 4.0 International license.

STAR Methods

Key resources table

REAGENT or RESOURCE	SOURCE	IDENTIFIER
Antibodies		
Rabbit polyclonal anti-Mic60	Cusabio	custom-made
Mouse monoclonal anti-MTCO1	Abcam	Cat# ab110270; RRID: AB_10863346
Mouse monoclonal anti-PGK1	Abcam	Cat# ab113687; RRID: AB_10861977
Mouse IgG HRP Linked Whole Antibody	Cytiva	Cat# GENA931-1ML
Rabbit IgG HRP Linked Whole Antibody	Cytiva	Cat# GENA934-1ML; RRID: AB_2722659
Bacterial and virus strains		
One Shot TOP10 Electrocompetent E. coli cells	Thermo Fisher	Cat #C404050
Biological samples		
Chemicals, peptides, and recombinant proteins		
Critical commercial assays		
QIAprep Spin Miniprep Kit	QIAGEN	Cat# 27104
Yeast Mitochondria Isolation Kit	Abcam	Cat# ab178779
Western Lightning Plus-ECL, Enhanced Chemiluminescence Substrate	Perkin Elmer	Cat# NEL105001EA
MasterPure Yeast DNA Purification Kit	Biosearch Technologies	Cat # MPY80200
Deposited data		
Raw and analyzed data	This paper	
Whole Genome Sequencing of yeast strains	This paper	
Experimental models: Cell lines		

bioRxiv preprint doi: https://doi.org/10.1101/2024.04.26.591372; this version posted April 29, 2024. The copyright holder for this preprint (which was not certified by peer review) is the author/funder, who has granted bioRxiv a license to display the preprint in perpetuity. It is made available under aCC-BY-NC-ND 4.0 International license.

Experimental models: Organisms/strains		
S288c DBY12045	Gift by L. Stirling Churchman[46].	
Oligonucleotides		
Primers for amplifying donor DNA, see Table S3	This paper	N/A
Primers for confirming CRISPR strains, see Table S3	This paper	N/A
Oligonucleotides to generate gRNA from plasmid, see Table S3	This paper	N/A
Donor DNA, see Table S3	This paper	N/A
gRNA, see Table S3	This paper	N/A
Recombinant DNA		
Plasmid: bRA66	Addgene	Cat# 100952
Software and algorithms		
AlphaFold2	Jumper et al.[47]	
ColabFold	Mirdita et al.[48]	https://colab.research.google.com/github/sokrypton/ColabFold/blob/main/AlphaFold2.ipynb
ConSurf	Landau et al.[44], Yariv et al.[45]	https://consurf.tau.ac.il/consurf_index.php
Integrated Genome Browser	Freese et al.[49]	https://bioviz.org/
MAFFT	Katoh et al.[50,51]	
PRANK	Löytynoja et al.[52]	
IQ-TREE	Minh et al.[53]	http://www.iqtree.org
UCSF ChimeraX	Resource for Biocomputing, Visualization, and Informatics, University of California, San Francisco[54]	https://www.cgl.ucsf.edu/chimerax/
PyMOL	The PyMOL Molecular Graphics System, Schrödinger, LLC	https://pymol.org/

bioRxiv preprint doi: https://doi.org/10.1101/2024.04.26.591372; this version posted April 29, 2024. The copyright holder for this preprint (which was not certified by peer review) is the author/funder, who has granted bioRxiv a license to display the preprint in perpetuity. It is made available under aCC-BY-NC-ND 4.0 International license.

Samtools/bcftools	Danecek et al.[55]	http://www.htslib.org/, https://samtools.github.io/bcftools/bcftools.html
BWA	Li et al.[56]	https://bio-bwa.sourceforge.net/
Python scripts for aligning paired-end illumine sequencing data onto a fasta-formatted reference genome	This paper	https://github.com/tribell4310/wgs_pipe
Python and R scripts for accelerating phylogenetic analysis	This paper	https://github.com/tribell4310/phylogenetics
Python script for graphing growth data	This paper	

Resource availability

Lead contact

Further information and requests for resources and reagents should be directed to and will be fulfilled by the lead contact, Luke H. Chao (chao@molbio.mgh.harvard.edu).

Materials availability

Plasmids and yeast strains generated in this study are available from the lead contact upon request.

Data and code availability

- Whole Genome Sequencing data and original western blot images to be made publicly available upon publication.
- All original code has been deposited at Github and is publicly available as of the date of publication. DOIs are listed in the key resource table.
- Any additional information required to reanalyze the data reported in this paper is available from the lead contact upon request.

Method details

Yeast Strains and Growth

All *S. cerevisiae* strains used in this work are derivatives of the S288c DBY12045[46] strain (kindly gifted by L. Stirling Churchman). A complete list of all yeast strains generated and used is included as Table S2.

bioRxiv preprint doi: https://doi.org/10.1101/2024.04.26.591372; this version posted April 29, 2024. The copyright holder for this preprint (which was not certified by peer review) is the author/funder, who has granted bioRxiv a license to display the preprint in perpetuity. It is made available under aCC-BY-NC-ND 4.0 International license.

For spot assays, yeast strains were first grown in YPD (1% yeast extract, 2% peptone, 2% glucose) or YPEG (1% yeast extract, 2% peptone, 2% ethanol, 3% glycerol) media at 30˚C to an OD_{600} of 0.2 to 0.3. Cells were pelleted by centrifugation at 6,000 x g for 2 min and resuspended in water to a final OD_{600} of 0.1. Each sample was 5-fold serially diluted in water to obtain cells with an OD_{600} value ranging from 0.1 to 6.4 x 10^{-6}, then transferred to YPEG or YPD agar plates using a multichannel pipette. Plates were incubated at 30°C, 25˚C, or 18°C and imaged at 24-hour intervals for 7 days.

For liquid growth assays, yeast strains were first grown in YPD at 30˚C to an OD_{600} of 11. Following centrifugation at 6,000 x g for 2 minutes, cell pellets were resuspended in 50 ml YPEG to a final OD_{600} of 0.4 and grown at 30˚C for 72 hours. 3 technical and 3 biological replicates (N=9) were grown for each strain. Measurements were taken at defined time points and analyzed using the matplotlib[57] and pandas[58] libraries in Python.

CRISPR/Cas9 Endogenous Genome Editing

Mic60 knockout (*mic60*Δ), Mitofilin knockout (*mitofilin*Δ) and chimeric yeast Mic60 strains expressing Mitofilin domains of other species or reconstructed ancestral Mitofilin domains were generated by CRISPR-Cas9 using the method by Levi and Arava[59]. Synthesized oligonucleotides (Integrated DNA Technologies) encoding the desired sgRNA sequence were cloned into the Cas9-encoding bRA66 plasmid (Addgene, 100952). Yeast strains were co-transformed with 500 ng of modified bRA66 plasmid (encoding Cas9 and sgRNA) and 5 ug of synthesized donor DNA (GenScript) using a lithium acetate/PEG-3350/heat-shock protocol described by Shaw *et al*[60]. All plasmids, sgRNAs and donor DNAs are listed in Table S3. Gene modifications were verified by whole genome sequencing.

Whole Genome Sequencing Analysis

Genomic DNA from each yeast strain was extracted using the MasterPure Yeast DNA Purification Kit (Biosearch Technologies) and sequenced with HiSeq 50 nt paired-

bioRxiv preprint doi: https://doi.org/10.1101/2024.04.26.591372; this version posted April 29, 2024. The copyright holder for this preprint (which was not certified by peer review) is the author/funder, who has granted bioRxiv a license to display the preprint in perpetuity. It is made available under aCC-BY-NC-ND 4.0 International license.

end reads (Illumina). Reads were aligned against the *S. cerevisiae* S288C genome (Genbank GCF_000146045.2) using bwa[56] and samtools/bcftools[55]. For chimeric constructs, custom reference genomes were produced by manually editing the *S. cerevisiae* S288C genome in fasta format. Aligned reads were visualized using Integrated Genome Browser[49]. Chromosomal coverage was assessed with custom python scripts, available in an open-source repository (https://github.com/tribell4310/wgs_pipe).

Immunoblot Analysis of Protein Localization

Expression and mitochondrial localization of Mic60 for all yeast strains were evaluated through antibody detection by immunoblotting of isolated mitochondria. Yeast strains were prepared and grown as described above for growth assays in liquid YPEG for 28 hours. After centrifugation at 1,500 x g for 5 minutes, mitochondria were isolated using the Yeast Mitochondria Isolation Kit (Abcam). Spheroblasts were homogenized by pushing 12 times through a 25G needle. For immunoblot analysis, the following antibodies were used: anti-Mic60 (custom-made, Cusabio), anti-MTCO1 as a mitochondrial marker (ab110270, Abcam) and anti-PGK1 as a cytosolic marker (ab113687, Abcam).

Ancestral Sequence Reconstruction

Ancestral reconstruction was carried out following the method of Prinston *et al.*[61]. Briefly, Mic60 sequences were curated from the InterPro database[62] (IPR019133) as well as through searches of NCBI GenBank[63] and Uniprot[64] using BLAST[65] and HMMER[66] algorithms. Searches returned >5,000 sequences, which were aligned with MAFFT[50]. Sequences with large insertions or deletions and sequences with greater than 96% pairwise sequence identity were eliminated immediately. This set of sequences (Table S4) was then whittled down to 69 (yeast-focused tree) or 62 (animal-focused tree) sequences that effectively represented the full phylogenetic diversity of the evolutionary space using custom python scripts, available in an open-source repository (https://github.com/tribell4310/phylogenetics). Seven amoebozoan and other non-opisthokont eukaryotic sequences were then added to the alignments for outgroup

bioRxiv preprint doi: https://doi.org/10.1101/2024.04.26.591372; this version posted April 29, 2024. The copyright holder for this preprint (which was not certified by peer review) is the author/funder, who has granted bioRxiv a license to display the preprint in perpetuity. It is made available under aCC-BY-NC-ND 4.0 International license.

rooting, and the sequences were re-aligned using PRANK[52]. The best-fit substitution model (Q.yeast[40,41] with allowed invariable sites (+I) and a discrete Gamma model of site heterogeneity[67] with four rate categories (+G4) for the yeast-focused tree; LG[68] with a four-class free-rate model[42,69] of site heterogeneity (+R4) for the animal-focused tree) was determined using MODELFINDER[70] according to Bayesian information criterion. Phylogeny construction and ancestral reconstruction were performed in IQ-TREE[53] using default settings. Branch supports were inferred using SH-like approximate likelihood ratio tests[71] in IQ-TREE. Tanglegram comparison of phylogenies with the Open Tree of Life[72] was performed using the rotl package[73], as well as custom R scripts made available in the above-referenced open-source repository. All alignment positions were reconstructed without regard to relatively unpopulated gap regions. Gaps were manually removed from the reconstructed sequences by comparing the reconstructions to their nearest-neighbor extant sequences using a parsimony approach similar in principle to Fitch's algorithm[74].

Structure Prediction and Analysis

Model predictions for all proteins shown were generated by AlphaFold2[47] using ColabFold v. 1.5.5[48]. All sequences used for protein predictions are listed in Table S1. Visual representations of protein structures were created and analyzed with UCSF ChimeraX (Resource for Biocomputing, Visualization, and Informatics, University of California, San Francisco)[54] and PyMOL (The PyMOL Molecular Graphics System, Version 2.5 Schrödinger, LLC). Protein folds were compared by superposition using the matchmaker[75] command in ChimeraX. Sequence conservation was mapped onto the structures using the ConSurf webserver[44,45].

Supplemental Information

See Supplemental Information file.

Tables S1-S4.

bioRxiv preprint doi: https://doi.org/10.1101/2024.04.26.591372; this version posted April 29, 2024. The copyright holder for this preprint (which was not certified by peer review) is the author/funder, who has granted bioRxiv a license to display the preprint in perpetuity. It is made available under aCC-BY-NC-ND 4.0 International license.

References

1. Rossmann, M.P., Dubois, S.M., Agarwal, S. & Zon, L.I. Mitochondrial function in development and disease. *Dis Model Mech* **14**(2021).
2. Cogliati, S., Enriquez, J.A. & Scorrano, L. Mitochondrial Cristae: Where Beauty Meets Functionality. *Trends Biochem Sci* **41**, 261-273 (2016).
3. Kondadi, A.K., Anand, R. & Reichert, A.S. Cristae Membrane Dynamics - A Paradigm Change. *Trends Cell Biol* **30**, 923-936 (2020).
4. Zick, M., Rabl, R. & Reichert, A.S. Cristae formation-linking ultrastructure and function of mitochondria. *Biochim Biophys Acta* **1793**, 5-19 (2009).
5. Spinelli, J.B. & Haigis, M.C. The multifaceted contributions of mitochondria to cellular metabolism. *Nature Cell Biology* **20**, 745-754 (2018).
6. Daems, W.T. & Wisse, E. Shape and attachment of the cristae mitochondriales in mouse hepatic cell mitochondria. *J Ultrastruct Res* **16**, 123-40 (1966).
7. Perkins, G. et al. Electron tomography of neuronal mitochondria: three-dimensional structure and organization of cristae and membrane contacts. *J Struct Biol* **119**, 260-72 (1997).
8. Frey, T.G. & Mannella, C.A. The internal structure of mitochondria. *Trends Biochem Sci* **25**, 319-24 (2000).
9. John, G.B. et al. The mitochondrial inner membrane protein mitofilin controls cristae morphology. *Mol Biol Cell* **16**, 1543-54 (2005).
10. Rabl, R. et al. Formation of cristae and crista junctions in mitochondria depends on antagonism between Fcj1 and Su e/g. *J Cell Biol* **185**, 1047-63 (2009).
11. Harner, M. et al. The mitochondrial contact site complex, a determinant of mitochondrial architecture. *Embo j* **30**, 4356-70 (2011).
12. Friedman, J.R., Mourier, A., Yamada, J., McCaffery, J.M. & Nunnari, J. MICOS coordinates with respiratory complexes and lipids to establish mitochondrial inner membrane architecture. *Elife* **4**(2015).
13. Guarani, V. et al. QIL1 is a novel mitochondrial protein required for MICOS complex stability and cristae morphology. *Elife* **4**(2015).
14. Anand, R., Strecker, V., Urbach, J., Wittig, I. & Reichert, A.S. Mic13 Is Essential for Formation of Crista Junctions in Mammalian Cells. *PLoS One* **11**, e0160258 (2016).
15. Zerbes, R.M., Höß, P., Pfanner, N., van der Laan, M. & Bohnert, M. Distinct Roles of Mic12 and Mic27 in the Mitochondrial Contact Site and Cristae Organizing System. *Journal of Molecular Biology* **428**, 1485-1492 (2016).
16. Muñoz-Gómez, S.A. et al. Intracytoplasmic-membrane development in alphaproteobacteria involves the homolog of the mitochondrial crista-developing protein Mic60. *Curr Biol* **33**, 1099-1111.e6 (2023).
17. von der Malsburg, K. et al. Dual Role of Mitofilin in Mitochondrial Membrane Organization and Protein Biogenesis. *Developmental Cell* **21**, 694-707 (2011).
18. Bohnert, M. et al. Role of mitochondrial inner membrane organizing system in protein biogenesis of the mitochondrial outer membrane. *Molecular Biology of the Cell* **23**, 3948-3956 (2012).
19. Ott, C. et al. Sam50 functions in mitochondrial intermembrane space bridging and biogenesis of respiratory complexes. *Mol Cell Biol* **32**, 1173-88 (2012).

bioRxiv preprint doi: https://doi.org/10.1101/2024.04.26.591372; this version posted April 29, 2024. The copyright holder for this preprint (which was not certified by peer review) is the author/funder, who has granted bioRxiv a license to display the preprint in perpetuity. It is made available under aCC-BY-NC-ND 4.0 International license.

20. Tang, J. et al. Sam50–Mic19–Mic60 axis determines mitochondrial cristae architecture by mediating mitochondrial outer and inner membrane contact. *Cell Death & Differentiation* **27**, 146-160 (2020).
21. Muñoz-Gómez, Sergio A. et al. Ancient Homology of the Mitochondrial Contact Site and Cristae Organizing System Points to an Endosymbiotic Origin of Mitochondrial Cristae. *Current Biology* **25**, 1489-1495 (2015).
22. Muñoz-Gómez, S.A., Wideman, J.G., Roger, A.J. & Slamovits, C.H. The Origin of Mitochondrial Cristae from Alphaproteobacteria. *Molecular Biology and Evolution* **34**, 943-956 (2017).
23. Tarasenko, D. et al. The MICOS component Mic60 displays a conserved membrane-bending activity that is necessary for normal cristae morphology. *J Cell Biol* **216**, 889-899 (2017).
24. Hoppins, S. et al. A mitochondrial-focused genetic interaction map reveals a scaffold-like complex required for inner membrane organization in mitochondria. *J Cell Biol* **195**, 323-40 (2011).
25. Friedman, J.R., Mourier, A., Yamada, J., McCaffery, J.M. & Nunnari, J. MICOS coordinates with respiratory complexes and lipids to establish mitochondrial inner membrane architecture. *eLife* **4**, e07739 (2015).
26. Tirrell, P.S., Nguyen, K.N., Luby-Phelps, K. & Friedman, J.R. MICOS subcomplexes assemble independently on the mitochondrial inner membrane in proximity to ER contact sites. *Journal of Cell Biology* **219**(2020).
27. Körner, C. et al. The C-terminal domain of Fcj1 is required for formation of crista junctions and interacts with the TOB/SAM complex in mitochondria. *Molecular Biology of the Cell* **23**, 2143-2155 (2012).
28. Zerbes, R.M. et al. Role of MINOS in Mitochondrial Membrane Architecture: Cristae Morphology and Outer Membrane Interactions Differentially Depend on Mitofilin Domains. *Journal of Molecular Biology* **422**, 183-191 (2012).
29. Eramo, M.J., Lisnyak, V., Formosa, L.E. & Ryan, M.T. The 'mitochondrial contact site and cristae organising system' (MICOS) in health and human disease. *The Journal of Biochemistry* **167**, 243-255 (2019).
30. Pernas, L. & Scorrano, L. Mito-Morphosis: Mitochondrial Fusion, Fission, and Cristae Remodeling as Key Mediators of Cellular Function. *Annu Rev Physiol* **78**, 505-31 (2016).
31. Van Laar, V.S., Otero, P.A., Hastings, T.G. & Berman, S.B. Potential Role of Mic60/Mitofilin in Parkinson's Disease. *Frontiers in Neuroscience* **12**(2019).
32. Schweppe, D.K. et al. Mitochondrial protein interactome elucidated by chemical cross-linking mass spectrometry. *Proc Natl Acad Sci U S A* **114**, 1732-1737 (2017).
33. Bock-Bierbaum, T. et al. Structural insights into crista junction formation by the Mic60-Mic19 complex. *Science Advances* **8**, eabo4946 (2022).
34. Hessenberger, M. et al. Regulated membrane remodeling by Mic60 controls formation of mitochondrial crista junctions. *Nature Communications* **8**, 15258 (2017).
35. Hochberg, G.K.A. & Thornton, J.W. Reconstructing Ancient Proteins to Understand the Causes of Structure and Function. *Annual Review of Biophysics* **46**, 247-269 (2017).

bioRxiv preprint doi: https://doi.org/10.1101/2024.04.26.591372; this version posted April 29, 2024. The copyright holder for this preprint (which was not certified by peer review) is the author/funder, who has granted bioRxiv a license to display the preprint in perpetuity. It is made available under aCC-BY-NC-ND 4.0 International license.

36. Kumar, S. et al. TimeTree 5: An Expanded Resource for Species Divergence Times. *Molecular Biology and Evolution* **39**(2022).
37. Körner, C. et al. The C-terminal domain of Fcj1 is required for formation of crista junctions and interacts with the TOB/SAM complex in mitochondria. *Mol Biol Cell* **23**, 2143-55 (2012).
38. Muñoz-Gómez, S.A. et al. Intracytoplasmic-membrane development in alphaproteobacteria involves the homolog of the mitochondrial crista-developing protein Mic60. *Current Biology* **33**, 1099-1111.e6 (2023).
39. Tarasenko, D. et al. The MICOS component Mic60 displays a conserved membrane-bending activity that is necessary for normal cristae morphology. *J Cell Biol* **216**, 889-899 (2017).
40. Minh, B.Q., Dang, C.C., Vinh, L.S. & Lanfear, R. QMaker: Fast and Accurate Method to Estimate Empirical Models of Protein Evolution. *Systematic Biology* **70**, 1046-1060 (2021).
41. Shen, X.-X. et al. Tempo and Mode of Genome Evolution in the Budding Yeast Subphylum. *Cell* **175**, 1533-1545.e20 (2018).
42. Soubrier, J. et al. The Influence of Rate Heterogeneity among Sites on the Time Dependence of Molecular Rates. *Molecular Biology and Evolution* **29**, 3345-3358 (2012).
43. Strassert, J.F.H., Irisarri, I., Williams, T.A. & Burki, F. A molecular timescale for eukaryote evolution with implications for the origin of red algal-derived plastids. *Nature Communications* **12**, 1879 (2021).
44. Landau, M. et al. ConSurf 2005: the projection of evolutionary conservation scores of residues on protein structures. *Nucleic Acids Res* **33**, W299-302 (2005).
45. Yariv, B. et al. Using evolutionary data to make sense of macromolecules with a "face-lifted" ConSurf. *Protein Sci* **32**, e4582 (2023).
46. Couvillion, M.T., Soto, I.C., Shipkovenska, G. & Churchman, L.S. Synchronized mitochondrial and cytosolic translation programs. *Nature* **533**, 499-503 (2016).
47. Jumper, J. et al. Highly accurate protein structure prediction with AlphaFold. *Nature* **596**, 583-589 (2021).
48. Mirdita, M. et al. ColabFold: making protein folding accessible to all. *Nature Methods* **19**, 679-682 (2022).
49. Freese, N.H., Norris, D.C. & Loraine, A.E. Integrated genome browser: visual analytics platform for genomics. *Bioinformatics* **32**, 2089-2095 (2016).
50. Katoh, K., Misawa, K., Kuma, K.i. & Miyata, T. MAFFT: a novel method for rapid multiple sequence alignment based on fast Fourier transform. *Nucleic Acids Research* **30**, 3059-3066 (2002).
51. Katoh, K. & Standley, D.M. MAFFT Multiple Sequence Alignment Software Version 7: Improvements in Performance and Usability. *Molecular Biology and Evolution* **30**, 772-780 (2013).
52. Löytynoja, A. Phylogeny-aware alignment with PRANK. *Methods Mol Biol* **1079**, 155-70 (2014).
53. Minh, B.Q. et al. IQ-TREE 2: New Models and Efficient Methods for Phylogenetic Inference in the Genomic Era. *Molecular Biology and Evolution* **37**, 1530-1534 (2020).

bioRxiv preprint doi: https://doi.org/10.1101/2024.04.26.591372; this version posted April 29, 2024. The copyright holder for this preprint (which was not certified by peer review) is the author/funder, who has granted bioRxiv a license to display the preprint in perpetuity. It is made available under aCC-BY-NC-ND 4.0 International license.

54. Pettersen, E.F. et al. UCSF ChimeraX: Structure visualization for researchers, educators, and developers. *Protein Sci* **30**, 70-82 (2021).
55. Danecek, P. et al. Twelve years of SAMtools and BCFtools. *Gigascience* **10**(2021).
56. Li, H. & Durbin, R. Fast and accurate short read alignment with Burrows-Wheeler transform. *Bioinformatics* **25**, 1754-60 (2009).
57. Hunter, J.D. Matplotlib: A 2D Graphics Environment. *Computing in Science & Engineering* **9**, 90-95 (2007).
58. pandas-dev/pandas: Pandas. ([object Object], 2024).
59. Levi, O. & Arava, Y. Expanding the CRISPR/Cas9 Toolbox for Gene Engineering in S. cerevisiae. *Curr Microbiol* **77**, 468-478 (2020).
60. Shaw, W.M., Khalil, A.S. & Ellis, T. A Multiplex MoClo Toolkit for Extensive and Flexible Engineering of Saccharomyces cerevisiae. *ACS Synthetic Biology* **12**, 3393-3405 (2023).
61. Prinston, J.E. et al. Ancestral Reconstruction Approach to Acetylcholine Receptor Structure and Function. *Structure* **25**, 1295-1302.e3 (2017).
62. Paysan-Lafosse, T. et al. InterPro in 2022. *Nucleic Acids Res* **51**, D418-d427 (2023).
63. Benson, D.A. et al. GenBank. *Nucleic Acids Research* **41**, D36-D42 (2012).
64. UniProt: the Universal Protein Knowledgebase in 2023. *Nucleic Acids Res* **51**, D523-d531 (2023).
65. Sayers, E.W. et al. Database resources of the national center for biotechnology information. *Nucleic Acids Res* **50**, D20-d26 (2022).
66. Finn, R.D., Clements, J. & Eddy, S.R. HMMER web server: interactive sequence similarity searching. *Nucleic Acids Res* **39**, W29-37 (2011).
67. Yang, Z. Maximum likelihood phylogenetic estimation from DNA sequences with variable rates over sites: Approximate methods. *Journal of Molecular Evolution* **39**, 306-314 (1994).
68. Le, S.Q. & Gascuel, O. An Improved General Amino Acid Replacement Matrix. *Molecular Biology and Evolution* **25**, 1307-1320 (2008).
69. Yang, Z. A space-time process model for the evolution of DNA sequences. *Genetics* **139**, 993-1005 (1995).
70. Kalyaanamoorthy, S., Minh, B.Q., Wong, T.K.F., von Haeseler, A. & Jermiin, L.S. ModelFinder: fast model selection for accurate phylogenetic estimates. *Nature Methods* **14**, 587-589 (2017).
71. Anisimova, M. & Gascuel, O. Approximate likelihood-ratio test for branches: A fast, accurate, and powerful alternative. *Syst Biol* **55**, 539-52 (2006).
72. Rees, J.A. & Cranston, K. Automated assembly of a reference taxonomy for phylogenetic data synthesis. *Biodivers Data J*, e12581 (2017).
73. Michonneau, F., Brown, J.W. & Winter, D.J. rotl: an R package to interact with the Open Tree of Life data. *Methods in Ecology and Evolution* **7**, 1476-1481 (2016).
74. Fitch, W.M. Toward Defining the Course of Evolution: Minimum Change for a Specific Tree Topology. *Systematic Zoology* **20**, 406-416 (1971).
75. Meng, E.C., Pettersen, E.F., Couch, G.S., Huang, C.C. & Ferrin, T.E. Tools for integrated sequence-structure analysis with UCSF Chimera. *BMC Bioinformatics* **7**, 339 (2006).

bioRxiv preprint doi: https://doi.org/10.1101/2024.04.26.591372; this version posted April 29, 2024. The copyright holder for this preprint (which was not certified by peer review) is the author/funder, who has granted bioRxiv a license to display the preprint in perpetuity. It is made available under aCC-BY-NC-ND 4.0 International license.